Journal of Biomedical Optics

SPIEDigitalLibrary.org/jbo

# Tissue surface as the reference arm in Fourier domain optical coherence tomography

Nikola Krstajić
Christian Tom A. Brown
Kishan Dholakia
Mario Ettore Giardini

SPIE

# Tissue surface as the reference arm in Fourier domain optical coherence tomography

**Nikola Krstajić,[a*] Christian Tom A. Brown,[b] Kishan Dholakia,[b] and Mario Ettore Giardini[c]**
[a]University of Edinburgh, School of Engineering, Institute for Integrated Micro and Nano Systems, Faraday Building, Kings Buildings, Mayfield Road, Edinburgh EH93JL, United Kingdom
[b]University of St. Andrews, SUPA School of Physics and Astronomy, North Haugh, St. Andrews KY16 9SS, United Kingdom
[c]University of St. Andrews, School of Medicine, North Haugh, St. Andrews KY16 9TF, United Kingdom

**Abstract.** We present a simple method applicable to common-path Fourier domain optical coherence tomography (OCT) in which the tissue surface is used as the reference arm. We propose using aluminium hydroxide powder as a potential tissue surface diffuser to allow wider application of this method. This technique allows one to avoid placing a reference arm reflective element, such as glass plate, on tissue, and intrinsically avoids both coherent and complex conjugate mirror artifacts associated with glass plates. Aluminium hydroxide can be sprayed onto tissue using spray nozzles commonly found in endoscopes. The sensitivity of the tissue reference arm common-path OCT image is 94 dB for a 50-$\mu$s charge-coupled device integration time, and 97.5 dB for a 200-$\mu$s CCD integration time.
 [DOI: 10.1117/1.JBO.17.7.071305]

Keywords: optical coherence tomography; common-path interferometry.

Paper 11567SS received Oct. 2, 2011; revised manuscript received Feb. 16, 2012; accepted for publication Feb. 22, 2012; published online May 15, 2012.

## 1 Introduction

Optical coherence tomography (OCT) is an imaging technique used to obtain cross-sectional views of tissues with a depth penetration of around 2 mm in scattering tissues such as skin, while in ophthalmology this depth is much higher.[1,2] Although realised two decades ago, it has only recently attained very high imaging speeds.[3] Efforts are underway to introduce OCT into clinical practice in other fields including endoscopy, dentistry and dermatology.

One problem facing an endoscopic implementation is the length of the optical fiber used in the sample arm. Usually the length needs to be greater than 2 m to provide a reasonable separation between the OCT instrumentation and the operating table. With such fiber lengths, dispersion and polarization matching become difficult due to dynamic effects of the fiber bending and the temperature variations along the length of the fiber. For example, the polarisation fading reduces fringe contrast,[4] and this is usually compensated by employing a polarisation controller. Environmental effects on fibers have been studied in detail by optical fiber sensors researchers over the last three decades.[5,6] In fact many ideas in low coherence interferometry have originated in fiber sensors research.[7] One solution to this problem is to employ common-path interferometry techniques.[8,9] In the published literature the term common-path interferometry is often referred to as self-referenced interferometry or reciprocal interferometry. In most cases, the common-path reference arm is formed by either the fiber tip[10–12] or by placing a eflective surface close to the tissue.[8,13] Alternatively, a mini-interferometer, comprising a beam-splitter, reference mirror and sample path, is mounted next to the fiber tip.[14,15] This implementation allows for the reference arm power to be optimised prior to scanning, thus maximising sensitivity.[16] Recently, multiple reflections within the sample arm were also used to implement a common-path OCT imaging system.[17,18]

In this article we present a simple and, to the best of our knowledge, novel way of acquiring common-path OCT images by using the tissue surface as the reflective surface of the reference arm. This removes the need for a separate reference reflective surface, such as glass plate. A glass plate has two surfaces, one of which is the reference arm while the other usually creates a horizontal coherent artefact and associated complex conjugate mirror artefact. Both artefacts are hard to remove.[13] Our technique can be applied to laparoscopy by employing a suitable spray nozzle within the endoscope. As both arms of the interferometer are placed on tissue, this architecture provides an interesting twist in interferometer configurations making it effectively a biological interferometer.

## 2 Materials and Methods

The Fourier domain optical coherence tomography (FDOCT) backscattered signal, $I_D$, is normally described as follows [Eq. (6.13) in Ref. 19]:

$$\begin{aligned}|\tilde{I}_D(\tau)| = I_0 \sum_i (|\rho_i|^2 + |\rho_R|^2) + \sum_{i,j,i\neq j} \{\rho_i \rho_j^* \Gamma[\tau - (\tau_i - \tau_j)]\} \\ + \sum_{i,j,i\neq j} \{\rho_i \rho_j^* \Gamma[\tau + (\tau_i - \tau_j)]\} \\ + \sum_i \{\rho_i \rho_R^* \Gamma[\tau - (\tau_i - \tau_R)]\} \\ + \sum_i \{\rho_i \rho_R^* \Gamma[\tau + (\tau_i - \tau_R)]\}, \end{aligned} \quad (1)$$

*Work presented was done while Nikola Krstajić was with the University of St. Andrews.

Address all correspondence to: Nikola Krstajić, University of Edinburgh, School of Engineering, Institute for Integrated Micro and Nano Systems, Faraday Building, Kings Buildings, Mayfield Road, Edinburgh EH93JL, United Kingdom. Tel: +01334461861; Fax: +44 (0)131 650 6554; E-mail: n.krstajic@physics.org

0091-3286/2012/$25.00 © 2012 SPIE

where $\rho_i$ and $\rho_j$ are the complex reflection coefficients of layers within the sample, while $\rho_R$ is the complex reflection coefficient of the reference arm. $\Gamma(\tau)$ is the coherence function of the source as a function of delay $\tau$, and $I_0$ is the incident intensity.

The first component in Eq. (1) is the intensity of the backscattered signal at $\tau = 0$ (DC term). In charge-coupled device (CCD) detectors this component cannot be removed, but it is removable in swept source OCT by using AC-coupled photodetectors. The second and third components are the autocorrelation term (describing sample signals interfering with each other) and its mirror image. The last two components provide the useful OCT signal and its mirror image.

Our approach places the "reference arm" physically on top of the sample. This can be interpreted as removing the last two terms of the equation above. We amplify the useful part of the autocorrelation signal that contains the structure of the sample by placing a thin layer of diffuse substance. Unwanted DC terms will potentially affect the top area of the resulting OCT image, but simple background subtraction can be employed to minimize this effect. Related work has been done in a patent detailing the use of a diffuse reference arm.[20] However, the autocorrelation signal, to the best of our knowledge, has not been demonstrated for structural imaging.

The FDOCT setup is shown in Fig. 1(a).[17] A superluminescent diode (SLED371-HP1, Superlum Diodes, Russia) illuminates the tissue via a 3-dB fiber coupler (FC850-40-50-APC, Thorlabs, NJ, USA) and microscope objective with a working distance of 25 mm and lateral resolution of 17 $\mu$m (LSM03-BB, Thorlabs, NJ, USA). The reference arm shares the physical path of the sample arm, and is generated by the diffuse surface on the top of the tissue. Due to its common-path configuration, the single mode fiber (SMF) used can be of arbitrary length. Backscattered spectra from the common arm are detected by a custom transmissive spectrograph, containing dispersive optics (volume phase holographic grating, 1200 $l$/mm, 830 nm, Wasatch Photonics, USA) and a line CCD detector (Aviiva EM1, part number EV71YEM1GE2014-BA9, 2048 pixels, pixel size 14 × 28 $\mu$m, e2v, United Kingdom). Custom software, which controls the acquisition from CCD, performs necessary signal processing and displays the image was written in NI Labwindows 2009 (National Instruments, Austin, Texas, USA). With a separate reference arm the OCT sensitivity was measured to be 100.1 dB at 50-$\mu$s CCD integration time. Measurement was performed by placing an optical-density 4 neutral density (ND) filter (ND40B, Thorlabs, NJ, USA) in the sample path, and using a mirror as the sample. At the wavelength range of interest, the double pass attenuation of the ND filter is 68 dB, and the signal level with this attenuation was measured to be 32.1 dB above noise. At 200-$\mu$s CCD integration time, the sensitivity was measured to be 103.5 dB. Common-path sensitivity measurements are described and discussed below. All acquired images presented in this article consist of 1024 A-scans.

We improve the common-path reference arm by applying a diffuse scatterer compound directly to the tissue surface [see Fig. 1(b)], thereby enhancing backscattering from the tissue surface. As a representative diffuse substance, we have chosen aluminium hydroxide (ATH). Aluminium, titanium, and barium oxides are well-known as scattering agents, and they have been widely used as low toxicity substances in near-infrared spectroscopy studies.[21]

The advantage of this common-path configuration is the tissue surface is the zero-path length reference point. Therefore, without any additional instrumental modification the arrangement naturally avoids complex conjugate mirror and coherent artefacts. Care should be taken to employ only a thin layer (<10 $\mu$m) of diffusive surface and provide high depth of field (DOF) focusing optics. We compare the images and reflection values for bare skin and skin covered in ATH. We also explain the image processing applied to images.

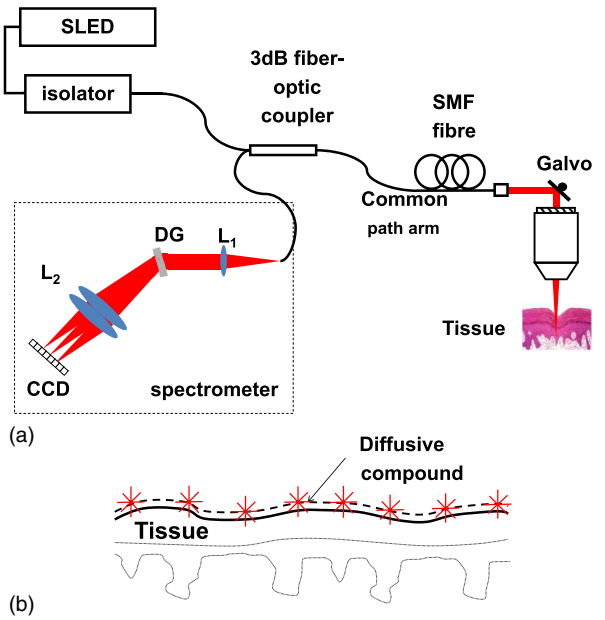


**Fig. 1** (a) FDOCT setup. (b) The diffuse reference surface is placed on top of the tissue analyzed. FDOCT: Fourier domain optical coherence tomography, DG: diffraction grating, $L_1$ and $L_2$: lenses, SLED: superluminescent diode, SMF: single mode fiber.

## 3 Results

A quick demonstration of tissue surface common-path OCT is shown in Fig. 2. The top image in Fig. 2 is the cross sectional image of onion skin without ATH while the bottom image has a thin layer of ATH applied. CCD integration time was set to 50 $\mu$s. Increased contrast is evident in the bottom image. Human tissue is more clinically relevant, so the remainder of the manuscript deals with human skin imaging.

Figure 3 demonstrates the imaging quality of tissue surface common-path OCT on skin. Figures 3(a) and 3(b) show the OCT images of skin at 50- and 200-$\mu$s CCD integration time where

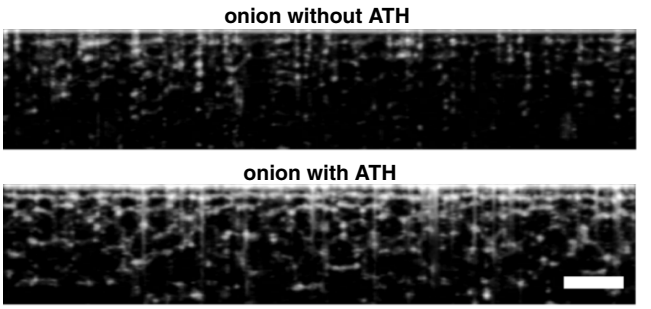


**Fig. 2** Top image is tissue surface common-path OCT of onion skin without ATH, while the bottom image has a thin layer of ATH added. The bar represents 0.5 mm. OCT: optical coherence tomography, ATH: aluminium hydroxide.

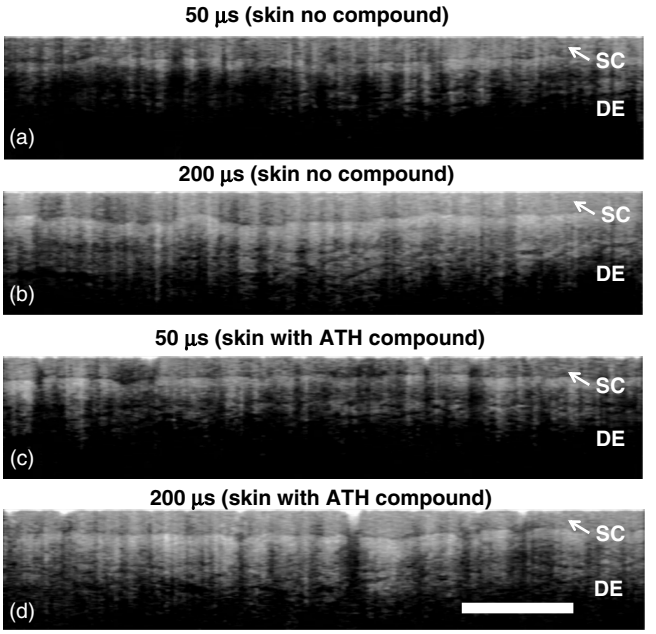


**Fig. 3** (a) and (b) show palmar finger skin images at 50- and 200-$\mu$s CCD integration times without any diffuse substance present on the surface. (c) and (b) show palmar finger skin images at 50- and 200-$\mu$s CCD integration times with a thin layer of ATH rubbed on the skin surface. The bar represents 1 mm. Tissue surface is located at the top edge of the images. ATH: aluminium hydroxide, SC: stratum corneum, DE: dermis.

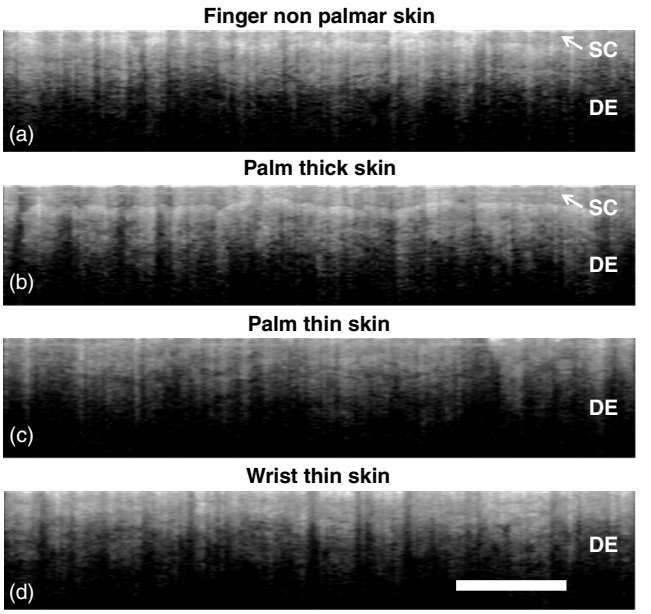


**Fig. 4** Imaging performance of the tissue surface common-path OCT at 200-$\mu$s CCD integration time and without any aluminium hydroxide (ATH) applied to surface. Various skin locations were chosen: (a) finger non palmar skin (b) palm thick skin (c) palm thin skin, and (d) wrist thin skin. Stratum corneum (SC) is clearly visible in (a) and (b), while it is too thin to be observed in (c) and (d). Thin dark stripes in the dermis (DE) are probably blood vessels. The white bar represents 1 mm.

inherent diffuse reflection of skin is used. Figures 3(c) and 3(d) show the OCT images of skin at 50 $\mu$s and 200-$\mu$s CCD integration time where ATH powder is mildly rubbed on the skin surface. In all cases, we image palmar finger skin. The images correspond to a similar area scanned, but the inevitable movement between scans introduces co-registration deviations. The images are affected by variation in intensity of each individual A-scan, and this has been compensated by band-pass filtering in the Fourier domain. Image processing details are provided further below.

The best quality is seen in Fig. 3(b) and 3(d) where dermal structures at a 1-mm depth can be seen. The quality in other images is also good, which indicates that inherent diffuse reflection of skin is often good enough. ATH improves image quality at 50-$\mu$s CCD integration time, while the advantage of using ATH at 200-$\mu$s CCD integration time is less obvious as both images [Fig. 3(b) and 3(d)] are of similar quality. During imaging, care was taken to have the specimen in focus as this provided the best imaging scenario. This optimizes the lateral resolution and increases the amount of backscatter from the tissue surface and underlying tissue. This is normal practice in any OCT imaging scenario. Note that although 200 $\mu$s may sound like a long integration time for an FDOCT system, it allows five frames per second acquisition (each with 1024 A scans). This is enough for most applications in minimally invasive surgery such as laparoscopy, where the surgeon would usually aim and scan a suspicious area within the visible lumen and instantly analyse the cross-sectional image.

When glycerol alone is applied to the tissue surface the images are of poorer quality than the ones displayed in Fig. 3. This is because of the known effect of glycerol to reduce diffuse reflection from the surface.[22] The images presented in Fig. 3 are effectively a fraction of the autocorrelation image one usually wants to remove. In other words, a fraction of the autocorrelation image is the sample surface interfering with structures beneath while the rest of the autocorrelation image is the sum of other layers interfering with each other. Therefore, an interesting corollary of this work is most of the autocorrelation image comes from the interference of the light reflected by the sample surface and the structures beneath. Thus, any optical clearing agent that reduces tissue scattering (such as glycerol) is likely to reduce the surface reflection, and thus the reference arm power in our arrangement.

Figure 4 shows images from other skin locations commonly investigated in dermatological practice. Images were acquired without applying ATH to the surface and at 200-$\mu$s CCD integration time. All images show dermal structures, probably blood vessels, up to about 900-$\mu$m deep. The stratum corneum is discernible in Fig. 4(a) (finger non-palmar skin) and 4(b) (palm thick skin). As expected, the stratum corneum is thicker in palmar skin than in non-palmar skin.

Figure 5 demonstrates the validity of our approach by overlaying the common-path OCT image derived from the tissue surface as reference arm with the OCT image obtained by using a separate reference arm. The image was taken in a single shot (50-$\mu$s CCD integration time), and dermal features in the common path OCT image correspond to dermal features in the normal OCT image. The normal OCT image has a sensitivity of 100.1 dB at 50-$\mu$s CCD integration time, so we can extrapolate the common-path image sensitivity by looking at the difference of reflectance in dB terms of equivalent tissue locations where the layers are flat. The difference of reflectance of equivalent locations is −3.14 dB when averaged over the middle of the OCT image in Fig. 5(a). Taking into account the signal fall-off in FDOCT of about 3 dB over 0.5 mm (approximate distance between equivalent tissue locations), the total difference in

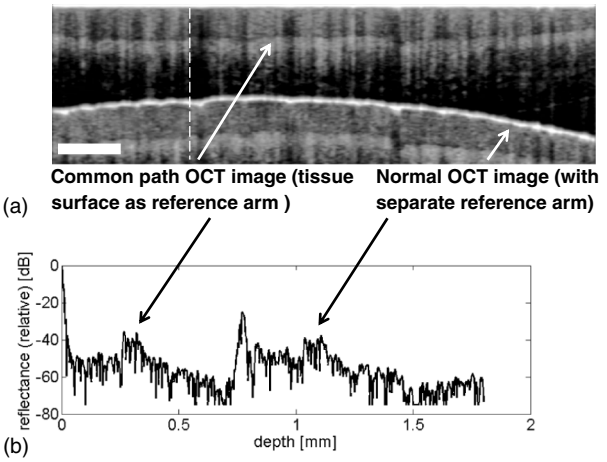


**Fig. 5** (a) Normal optical coherence tomography (OCT) image with separate reference arm overlaid with common path OCT image with tissue surface as the reference arm. White arrows point to common-path OCT image and normal OCT image respectively. The white bar represents 0.5 mm. (b) Line profile across the region with dashed line shown in (a). Dark arrows point to the lower layers of epidermis in the common-path OCT (the top section of the line profile) and the normal OCT (middle section of the line profile).

reflectance is approximately 6 dB. The normal OCT image therefore has 6-dB higher sensitivity than the common-path OCT image, so the sensitivity of the common-path image is 94 dB at 50-$\mu$s CCD integration time. The same measurement at 200-$\mu$s CCD integration time resulted in 103.5 dB sensitivity of the normal OCT image, and 97.5 dB of the common-path OCT image.

Often the difference is negligible as shown in Fig. 5(b) where lower epidermis pointed to by the dark arrows has the same reflectance in both common-path OCT and normal OCT. In this case, following Eq. (1) tissue surface has weaker reflection than the reference arm mirror by 3 dB taking into account the signal fall-off.

The remaining issue to resolve is to determine the anisotropy of ATH and other powders once placed on skin or other tissue. Our experience is that placing ATH powder directly onto skin has consistently improved images at low CCD integration times. Our experiments so far in combining ATH with a dispersing medium (e.g. Vaseline) have been unsuccessful due to index matching of ATH and the surrounding matrix, as this reduced the scattering properties of ATH. We are, however, confident this issue may be overcome by an appropriate combination of powder and dispersing medium.

All tissue reference arm images shown so far have been image-processed to remove vertical stripes (e.g. see the top image in Fig. 6). These appear due to variation in A-scan intensity during the scan. These are, in turn, due to random jumps and falls in back-reflected light intensity that are result of the corrugated surface of skin. The skin surface has been described as quasi-random periodic surface and simulations of back-reflection spectra were found to match experimental results.[23] Surface roughness has also been shown to affect severely the optical properties of tissue.[24] This partially explains why optical clearing with glycerol improves OCT images in systems with a separate reference arm.[22] OCT images of skin obtained with a separate reference arm also have the vertical stripes, but they are less pronounced as the reference arm power remains the same while in our case this varies.

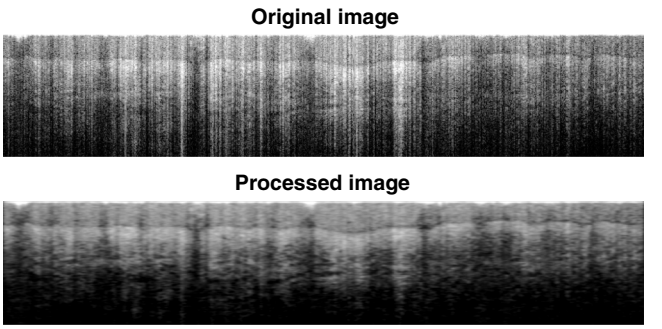


**Fig. 6** Image processing is applied to acquired image (top) to reduce noise and vertical stripes in the resulting image (bottom).

A simple method was developed to remove them. Each image acquired was processed by a Fast Fourier Transform (FFT) band-pass Butterworth filter (see, for example, Chapter 4 in Ref. 25). The filter was set to resolve features between 30 and 1 mm in size, and higher spatial frequencies were attenuated. Vertical stripes were eliminated by attenuating DC values along the $x$-axis in the Fourier domain. The bottom image in Fig. 6 is a much improved version, and dermal vasculature is clearer.

Figure 7 compares the surface reflectance of skin from two images acquired where one was with ATH while the other was without ATH. By examining the surface reflectance values in both cases we can evaluate the advantages of using ATH or similar compounds. In order for comparison to be valid, both images had to have the same focusing conditions. This was performed by acquiring the normal OCT image overlaid such as the one shown in Fig. 5. Reflectance was compared only if the normal OCT images were at the same distance from the top (zero path length), thus maintaining strict focus conditions. The values were obtained by averaging reflectance for 1024 A-scans for each image. The error bars were obtained by calculating the standard deviation for each depth over all 1024 A-scans. The background spectrum due to fiber-end reflection was subtracted prior to imaging. CCD integration time was set to 100 $\mu$s. Figure 7 shows that skin with ATH has a higher reflectance by >5 dB, and is therefore better suited as the reflector for common-path OCT reference arm. Another interesting observation is employing ATH causes a higher variation in reflectance; error bars are much larger for skin with ATH. This can be expected

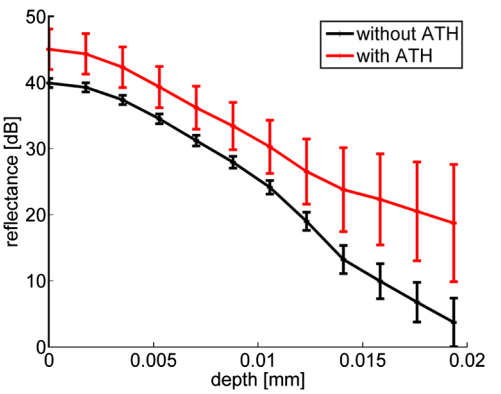


**Fig. 7** Relative comparison of reflectance (in dB levels) at the top 20 $\mu$m of the optical coherence tomography (OCT) image of skin with aluminium hydroxide (ATH) and without ATH. Reflectance of skin is increased with ATH. Also, ATH increases the variability in skin reflectance as indicated by the error bars.

from the discussion related to skin anatomy and image processing mentioned above. The question remains—why the increase in reference arm power by applying ATH powder does not result in better ATH images in Fig. 3 for slower integration times, i.e. 200 $\mu$s. One possibility is the reference arm spectrum is unavoidably noisy because of the diffuse nature of surface reflection. This in turn may affect the point-spread function of OCT imaging.[26]

## 4 Discussion

Although common-path techniques automatically compensate for dispersion mismatch and polarization fading, the image quality presented in the published literature is generally lower than that obtained in standard two-arm Michelson interferometers. For example, this is apparent if we compare the excellent skin images obtained in Ref. 27 with common-path images in Ref. 17. In this comparison we limited ourselves to true common-path OCT systems, which do not include a mini-interferometer at the tip of the fiber. We believe the method presented here significantly advances common-path techniques by providing a much improved image quality. One can envisage using tissue-friendly compounds for imaging internal organs in this manner. In all implementations of this technique it will be important to maintain a constant distance between the focusing optics and the tissue[28] in order to optimize tissue reflectance and lateral resolution. In all variants of OCT set-ups, the sample should be in close focus. Specific to our common-path arrangement is that, unless the surface is kept in the focal point of the objective, confocal rejection will attenuate the surface reflection, thereby reducing the reference intensity and the sensitivity. However, this is not a substantial effect for high depth-of-field microscope objectives. For example, consider the objective used in this study LSM-03BB (Thorlabs), which has 17-$\mu$m spot size. If the tissue surface is 1 mm away from focus, the reflectance will be attenuated by 3 dB which in turn reduces sensitivity by the same amount. These values were derived by calculating the confocal function for the objective used at a wavelength of 840 nm.[29] Another possible drawback of this technique is the top-surface topology is not visible as it appears flattened at the top of the image. Consequently, inner structures are geometrically distorted for curved surfaces. Despite a strong diffuser being present on top of the tissue, the underlying structures are still clearly visible.

Toxicity of ATH and related powders is an important issue as well. Although an inert substance, the toxicity of ATH as the scattering agent for endoscopy applications remains to be evaluated. The ceramic form of ATH (alumina) has been used as the biocompatible material for hip prostheses[30,31] for several decades. Hip prostheses release debris with time, and these seem to be absorbed by the body without much difficulty. Even if ATH is found to be overly toxic, numerous alternative scattering contrast agents are possible,[32] including substances such as gold nanoparticles[33] which can be used to enhance complementary spectroscopic signals, e.g. surface enhanced Raman scattering.[34]

## 5 Conclusion

We have shown a novel common-path mode of imaging tissue in OCT. The tissue surface of interest is used as the reflector for the common path. We have also shown that sensitivity may be increased through the application of diffuse compounds to the surface of the tissue. The method naturally avoids the complex conjugate mirror and coherent artifacts present when glass plate is used. It opens up a new approach to OCT imaging in which an optical diffuse compound is applied on the tissue surface. The sensitivity of the tissue surface reference OCT was found to be 6 dB less than the sensitivity of normal OCT (i.e. where the reference arm power is optimized for maximum sensitivity). Future work will focus on combining the diffuse substance such as ATH, with a dispersing matrix, eventually with an additional optical tissue clearing effect to provide better depth penetration while keeping the surface optically diffuse.

### Acknowledgments

This work has been funded by European Union FP7 project ARAKNES (www.araknes.org) under Grant Agreement No. 224565. Kishan Dholakia is a Royal Society Wolfson Research Merit Award holder. Intellectual property rights on this work are covered by the University of St. Andrews. Nikola Krstajić (NK) wishes to thank Cathy Shields for reviewing the manuscript. Significant sections of OCT software were written while NK was employed by the University of Sheffield. NK wishes to thank Dr. Steve Matcher and his group at the University of Sheffield for all their help in learning OCT techniques.

### References

1. W. Drexler and J. G. Fujimoto, *Optical Coherence Tomography: Technology and Applications, Illustrated* Ed., Springer, Heidelberg, Germany (2008).
2. M. E. Brezinski, *Optical Coherence Tomography: Principles and Applications*, 1st ed, Academic Press, Burlington, MA, USA (2006).
3. M. Wojtkowski, "High-speed optical coherence tomography: basics and applications," *Appl. Opt.* **49**(16), D30–D61 (2010).
4. D. W. Stowe, D. R. Moore, and R. G. Priest, "Polarization fading in fiber interferometric sensors," *IEEE Trans. Microw. Theor. Tech.* **30**(10), 1632–1635 (1982).
5. K. T. V. Grattan and T. Sun, "Fiber optic sensor technology: an overview," *Sensor Actuator Phys.* **82**(1–3), 40–61 (2000).
6. E. Udd, "An overview of fiber optic sensors," *Rev. Sci. Instrum.* **66**(8), 4015–4030 (1995).
7. A. G. Podoleanu, "Fiber optics, from sensing to non invasive high resolution medical imaging," *J. Lightwave Technol.* **28**(4), 624–640 (2010).
8. A. B. Vakhtin et al., "Common-path interferometer for frequency-domain optical coherence tomography," *Appl. Opt.* **42**(34), 6953–6958 (2003).
9. J.-U. Kang et al., "Common-path optical coherence tomography for biomedical imaging and sensing," *J. Opt. Soc. Korea* **14**(1), 1–13 (2010).
10. J. Bush, "All-fiber optic coherence domain interferometric techniques," *Proc. SPIE* **4204**, 71–80 (2001).
11. A. D. Drake and D. C. Leiner, "Fiber optic interferometer for remote subangstrom vibration measurement," *Rev. Sci. Instrum.* **55**(2), 162–165 (1984).
12. K. M. Tan et al., "In-fiber common-path optical coherence tomography using a conical-tip fiber," *Opt. Express* **17**(4), 2375–2384 (2009).
13. A. R. Tumlinson et al., "Endoscope-tip interferometer for ultrahigh resolution frequency domain optical coherence tomography in mouse colon," *Opt. Express* **14**(5), 1878–1887 (2006).
14. R. A. Leitgeb et al., "Complex ambiguity-free fourier domain optical coherence tomography through transverse scanning," *Opt. Lett.* **32**(23), 3453–3455 (2007).
15. P. Cimalla et al., "Simultaneous dual-band optical coherence tomography in the spectral domain for high resolution in vivo imaging," *Opt. Express* **17**(22), 19486–19500 (2009).
16. R. Leitgeb, C. Hitzenberger, and A. Fercher, "Performance of fourier domain vs. time domain optical coherence tomography," *Opt. Express* **11**(8), 889–894 (2003).
17. N. Krstajić, R. Hogg, and S. J. Matcher, "Common path fourier domain optical coherence tomography based on multiple reflections within the sample arm," *Opt. Commun.* **284**(12), 3168–3172 (2011).

18. N. Krstajić et al., "Common path Michelson interferometer based on multiple reflections within the sample arm: sensor applications and imaging artefacts," *Meas. Sci. Technol.* **22**(2), 027002 (2011).
19. R. A. Leitgeb and M. Wojtkowski, "Complex and coherence noise free fourier domain optical coherence tomography," in *Optical Coherence Tomography*, W. Drexler and J. G. Fujimoto, Eds., Springer, Berlin Heidelberg, pp. 177–207 (2008).
20. F. Feldshtein and P. Amazeen, "Common path systems and methods for frequency domain and time domain optical coherence tomography using non-specular reference reflection and a delivering device for optical radiation with a partially optically transparent non-specular reference reflector," U. S. Patent No. 7,821,643 (2010).
21. B. W. Pogue and M. S. Patterson, "Review of tissue simulating phantoms for optical spectroscopy, imaging and dosimetry," *J. Biomed. Opt.* **11**(4), 041102 (2006).
22. G. Vargas et al., "Use of an agent to reduce scattering in skin," *Lasers Surg. Med.* **24**(2), 133–141 (1999).
23. I. V. Meglinski and S. J. Matcher, "Quantitative assessment of skin layers absorption and skin reflectance spectra simulation in the visible and near-infrared spectral regions," *Physiol. Meas.* **23**, 741–753 (2002).
24. X. Ma, J. Q. Lu, and X.-H. Hu, "Effect of surface roughness on determination of bulk tissue optical parameters," *Opt. Lett.* **28**(22), 2204–2206 (2003).
25. R. C. Gonzalez and P. Wintz, Chapter 4 in *Digital Image Processing*, 2nd Revised ed., Longman Higher Education, MA, USA (1987).
26. C. Akcay, P. Parrein, and J. P. Rolland, "Estimation of longitudinal resolution in optical coherence imaging," *Appl. Opt.* **41**(25), 5256–5262 (2002).
27. A. Alex et al., "Multispectral in vivo three-dimensional optical coherence tomography of human skin," *J. Biomed. Opt.* **15**, 026025 (2010).
28. K. Zhang et al., "A surface topology and motion compensation system for microsurgery guidance and intervention based on common-path optical coherence tomography," *IEEE Trans. Biomed. Eng.* **56**(9), 2318–2321 (2009).
29. B. E. A. Saleh and M. C. Teich, Chapter 3 in *Fundamentals of Photonics*, 2nd ed., Wiley-Blackwell, Hoboken, NJ, USA (2007).
30. P. Zeng, "Biocompatible alumina ceramic for total hip replacements," *Tribol. Mater. Surface. Interfac.* **2**(2), 109–120 (2008).
31. G. Willmann, "Ceramics for total hip replacement—what a surgeon should know," *Orthopedics* **21**(2), 173–177 (1998).
32. S. A. Boppart et al., "Optical probes and techniques for molecular contrast enhancement in coherence imaging," *J. Biomed. Opt.* **10**(4), 41208 (2005).
33. C. J. Murphy et al., "Gold nanoparticles in biology: beyond toxicity to cellular imaging," *Acc. Chem. Res.* **41**(12), 1721–1730 (2008).
34. M. A. Ochsenkuhn et al., "Nanoshells for surface-enhanced raman spectroscopy in eukaryotic cells: cellular response and sensor development," *ACS Nano.* **3**(11), 3613–3621 (2009).